2 USER TECHNICAL SUPPORT

2.1 Insertion Devices

Since the last *Experimental Facilities Division/User Program Division Technical Progress Report* (ANL/APS/TB-38, 2000), the Insertion Device Group (newly renamed the Magnetic Devices Group) has begun to deal with radiation damage to insertion devices (IDs). As routine use of top-up mode began, a decrease in the field strength of permanent magnets in the IDs with the highest dose rate is being seen. Significant damage levels are so far limited to sector 3, where the first small-aperture vacuum chamber downstream of injection is located. Devices from that and other sectors are being removed, retuned, and reinstalled during the shutdowns, both to keep the sector 3 users provided with acceptably operating IDs and to assess the damage elsewhere. Planned new dosimetry techniques have now been implemented, and additional shielding is being added.

A prototype for the undulators that will be built for the LCLS project has been assembled and is undergoing tuning and testing at APS. One goal is to search for possible economies in the production of the 33 undulators that will be needed for the Linac Coherent Light Source (LCLS).

Improvements have also been made to the ID magnetic measurement facility. Control systems have been updated with new hardware to replace obsolete components, and the software has been rewritten. An advantage of the new hardware is a significant reduction in the electronic noise levels, by eliminating the long wires to the motors, which contributed much of the noise in the Hall probe readings.

2.1.1 Dosimetry

At the APS concern for radiation damage of the IDs and other critical components has led to systematic dose monitoring at those components.

The IDs are subjected to a harsh radiation environment that can lead to radiation-induced demagnetization. This radiation environment is primarily composed of gamma rays, x-rays, electrons and neutrons.

Systematic dose monitoring on the IDs is used to determine the dose distribution profiles around the storage ring and the FEL, and regions where the probability of damage is highest. Integrated doses on the IDs also provide information on the magnitude of the damage threshold.

In addition, other critical components around the facility (such as CCD cameras, encoders, motors and cables) suffer from radiation aging. Integrated radiation dose measurements for these components give an indication of their radiation sensitivity and their lifetime in the APS radiation environment.

A dosimetry system would ideally exhibit radiation energy and radiation quality independent response in the radiation environment of interest. An additional requirement is a broad useful dose range. However, due to the broad spectrum of radiation energies, multiple radiation qualities, and very broad dose ranges around synchrotron facilities such a requirement can only be partially satisfied.

To date, dose monitoring at APS has been performed with LiF and $Li_2B_4O_7$:Mn TLDs

(thermoluminescent dosimeters) and radiachromic films. In addition, in 2002 a new high dose dosimetry technique has been added: alanine electron paramagnetic resonance (EPR) dosimetry. All these dosimetry techniques are tissue equivalent.

Alanine is an amino acid where the disrupted molecular bonding due to ionizing radiation gives rise to free radicals. The number of free, stable radicals is a function of the absorbed dose. The radical concentration can then be analyzed with EPR. Alanine dosimetry exhibits equivalent response for photons and electrons, and negligible temperature and humidity coefficients. In addition, it exhibits energy independent response above approximately 100 keV; however, dose underestimation occurs for photon energies below that value.

The EPR spectrometer is an e-scan Bruker analyzer that is suitable for both pellet and film alanine dosimetry and capable of providing dose measurements from 1 krad to 20 Mrad. The dosimeters used currently at the APS are alanine films with a saturation point equal to 50 Mrad.

Dosimetry measurements on the IDs have, so far, been performed on the upstream (US) and downstream (DS) ends of the devices. An effect on the absorbed doses is from the gap-size history during ID operation; maximum gap reduces the synchrotron background while it also allows for potential scattering of bremsstrahlung radiation in less critical directions. Currently the minimum gap on most IDs is 11 mm while the maximum gap is equal to 180 mm.

The US doses are also being affected by the absence or presence of shielding upstream of the IDs; a few IDs are not shielded due to space constraints. In addition, the absorbed doses are affected by nonuniformities in the vacuum and temperature profiles around the storage ring, and the current present in the ring. The storage ring lattice being used also affects the dose. Lattices with short lifetimes can be and are used during top-up operation; the short lifetime means a higher dose.

The TLD–800's ($Li_2B_4O_7$:Mn TLD's) were inserted in the storage ring for the first time during the run 2001-3 (Fig. 2.1) During that run they registered doses over 1 Mrad at the DS ends of many IDs, with the highest doses at the IDs in sector 3, APS27#2 and U27#12. The useful dose range of the TLD-800 extends up to approximately 10^7 rad.

Alanine dosimeters were inserted for the first time in the storage ring in 2002. The absorbed doses during run 2002-2 are shown in Fig. 2.2. High absorbed doses were again recorded on the IDs in sector 3. This is primarily due to an increased probability for non-gas bremsstrahlung following recent installation of a smaller aperture ID vacuum chamber in that sector. The recorded doses are higher in the DS end of the devices. The DS doses remained below approximately 1 Mrad while the US doses remained below approximately 100 krad on most other IDs.

To date, the potential for radiation damage appears to be highest in sector 3. Due to the radiation-induced demagnetization already observed in both U27#12 and APS27#2, those alanine dosimeters are now being replaced as often as machine intervention schedules allow so that changes to the dose rate can be detected more promptly. Dosimeters in the other sectors are being replaced at the end of each run (i.e., at approximately 3 month time intervals).

Additional shielding is being inserted in sector 3 in an attempt to reduce the dose to the IDs. In addition, temperature is being

monitored along the length of the IDs that suffered radiation-induced demagnetization.

During upcoming shutdowns IDs will be removed from the storage ring and checked for potential radiation damage. The IDs will be selected based partly on integrated dose results. In addition, IDs where significantly high absorbed doses were observed during one run (such as U33#30 in sector 22, Fig. 2.2) will also be examined for potential radiation damage.

The contribution to the total absorbed dose from synchrotron radiation, bremsstrahlung radiation and the associated photoneutron component need also to be evaluated for a better interpretation of the dosimetry results. Such calculations are planned for the APS radiation environment. In addition, the simultaneous use of different dosimetry techniques can potentially provide a better characterization of the radiation field and dose profile around the facility.

The response of the dosimeters at cryogenic temperatures is also of interest due to the potential addition of superconducting cavities at the APS. The response of alanine dosimeters in this temperature regime is quite well known. The relative response of the dosimeters at cryogenic temperatures for the dosimeters currently being used at the APS is being examined.

Future dosimetry plans also involve dosimetry intercomparison studies between APS and other accelerator facilities.

Routine dose monitoring on the IDs at the APS is critical; however, the primary focus of the radiation damage studies is a better understanding of the damage process so that efficient techniques can be developed to prevent the damage.

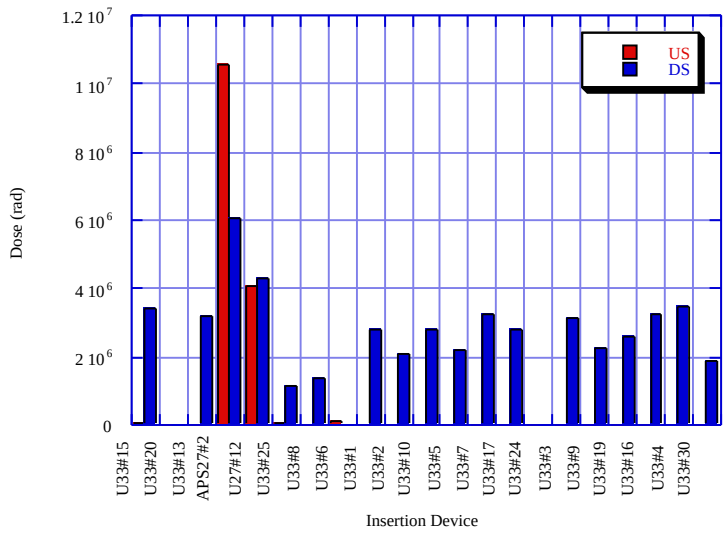

Fig. 2.1. Absorbed dose on the IDs recorded by TLD-800 dosimeters during run 2001-3.

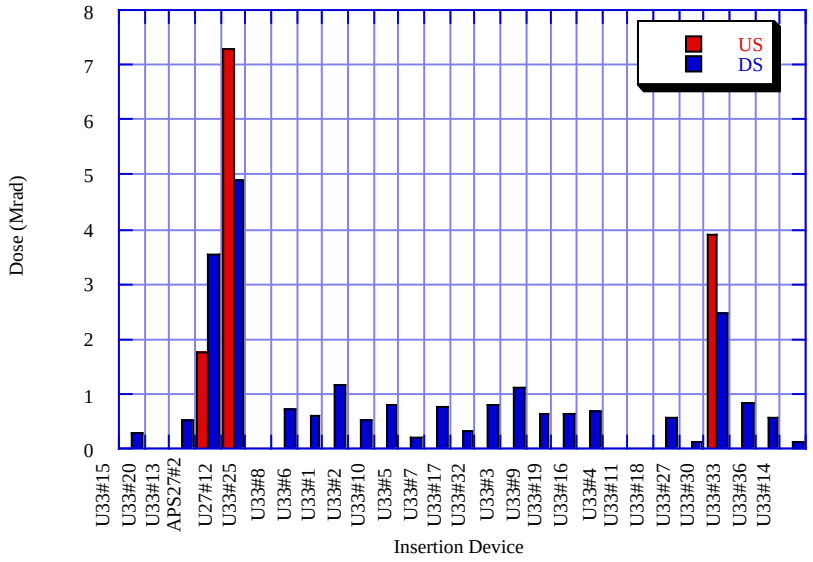

Fig. 2.2. Absorbed dose on the IDs recorded by alanine dosimeters during run 2002-2.

2.1.2 Radiation-Induced Damage to IDs

Damage has now been observed in a few IDs at the APS. During the August-September 2001 run, the APS was run in top-up mode for much of the run. In addition, a new low-emittance lattice was being used, and the injection efficiency had not yet been optimized for these new conditions. The smallest aperture in the ring is a 5-mm-aperture insertion device vacuum chamber, and the first such chamber after the injection point is located in sector 3. It is suspected that much of the beam that was lost during injection was lost there. Abnormally high doses were recorded by radiation dosimeters placed on the upstream and downstream end of the IDs in that sector. This prompted the removal of these devices from the storage ring during the December-January shutdown to check them for radiation damage.

As can be seen in Figs. 2.3 and 2.4, radiation-induced demagnetization was observed for both IDs, with the damage being more pronounced for the downstream U27#12. The performance of both devices was significantly impaired.

Monitoring of the dose to these devices continued during the Jan.-Apr. 2002 run, and the dose continued to be high, particularly for the downstream device. During the May 2002 shutdown, the downstream device, U27#12, was again removed to be rechecked, and more damage was found, as can be seen in Fig. 2.5.

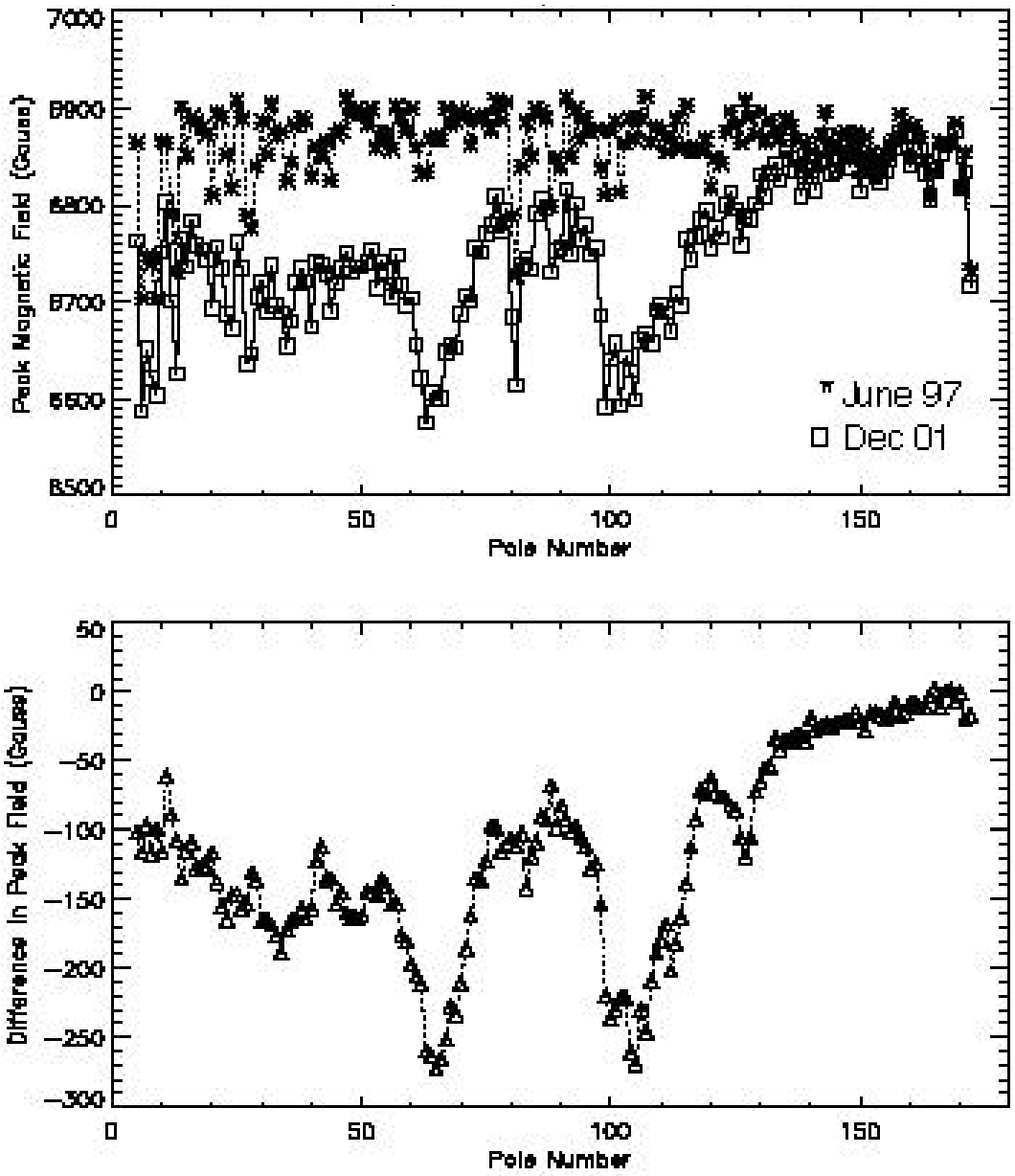

Fig. 2.3. Magnetic field changes in the downstream undulator in sector 3, U27#12, at 10.5 mm gap. The top panel shows the peak magnetic field under each pole as measured in June 1997 (before the device was installed) and in Dec. 2001. The damage is small at the upstream end on the right. The bottom panel shows the difference in the magnetic field. (The data for the weaker end poles are omitted.)

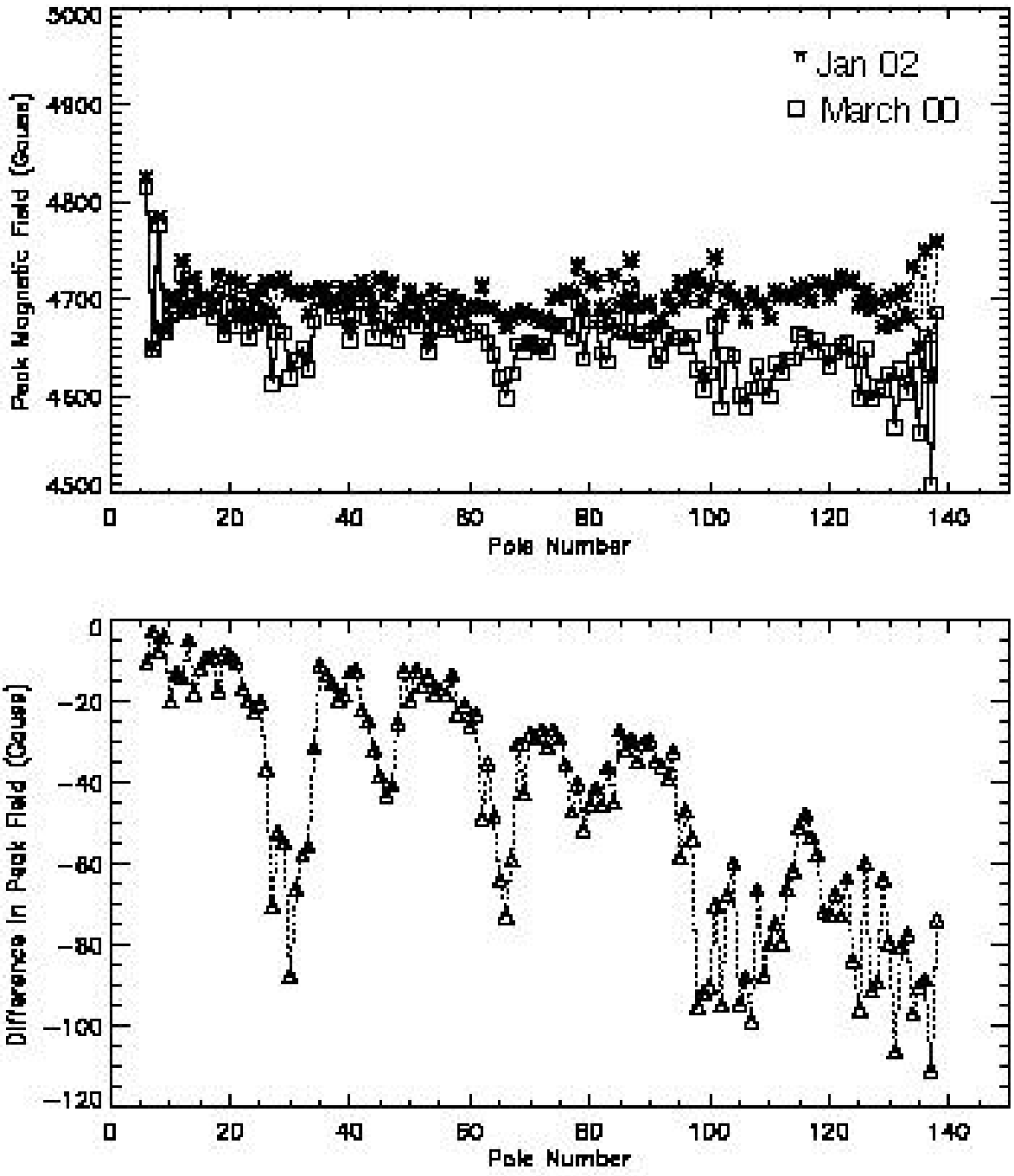

Fig. 2.4. Magnetic field changes in the upstream undulator in sector 3, APS27#2, at 11.5 mm gap. The top panel shows the peak magnetic field under each pole as measured in March 2000 (before the device was installed) and in Dec. 2001. The damage is larger at the upstream end (on the right), in contrast to the damage to the downstream undulator. The bottom panel shows the difference in the magnetic field. (The data for the weaker end poles are omitted.)

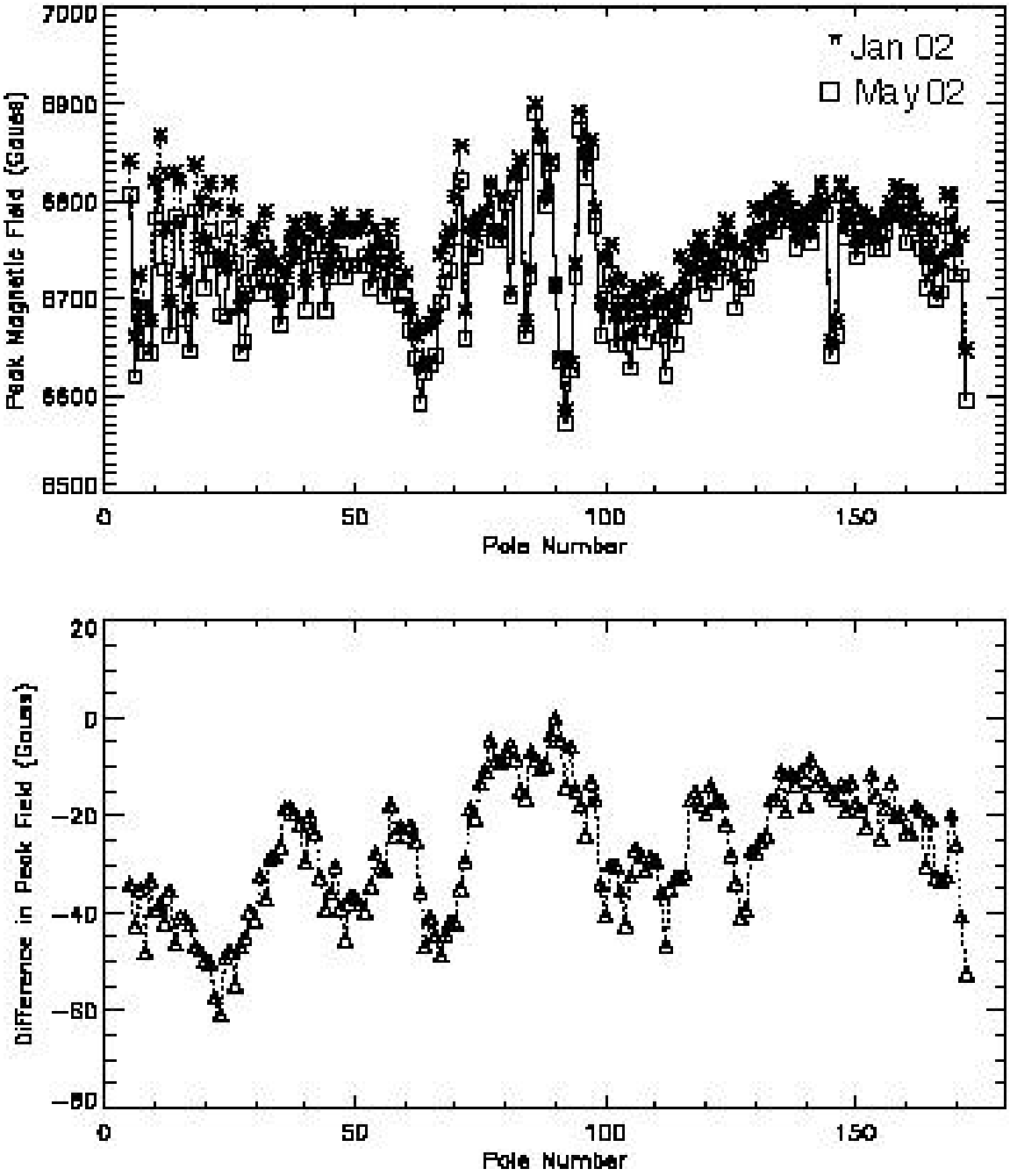

Fig. 2.5. Magnetic field changes in the downstream undulator in sector 3, U27#12, at 10.5 mm gap. The top panel shows the peak magnetic field under each pole as measured in Jan. 2002, after the device had been retuned, and in May 2002. The bottom panel shows the difference in the magnetic field. (The data for the weaker end poles are omitted.) The damage is less than that found previously, but clearly damage is continuing.

Two other IDs were also removed in May 2002 for checking. One was found to be slightly damaged, as can be seen in Fig. 2.6. The other does not show radiation damage (Fig. 2.7), though there is a uniform increase in the strength of the magnetic field. This uniform change in the field can be attributed either to the fact that a smaller Hall probe was used that averages the peak field over a smaller area, thereby giving a higher peak reading, or to backlash in the gap-setting mechanism that was not properly removed.

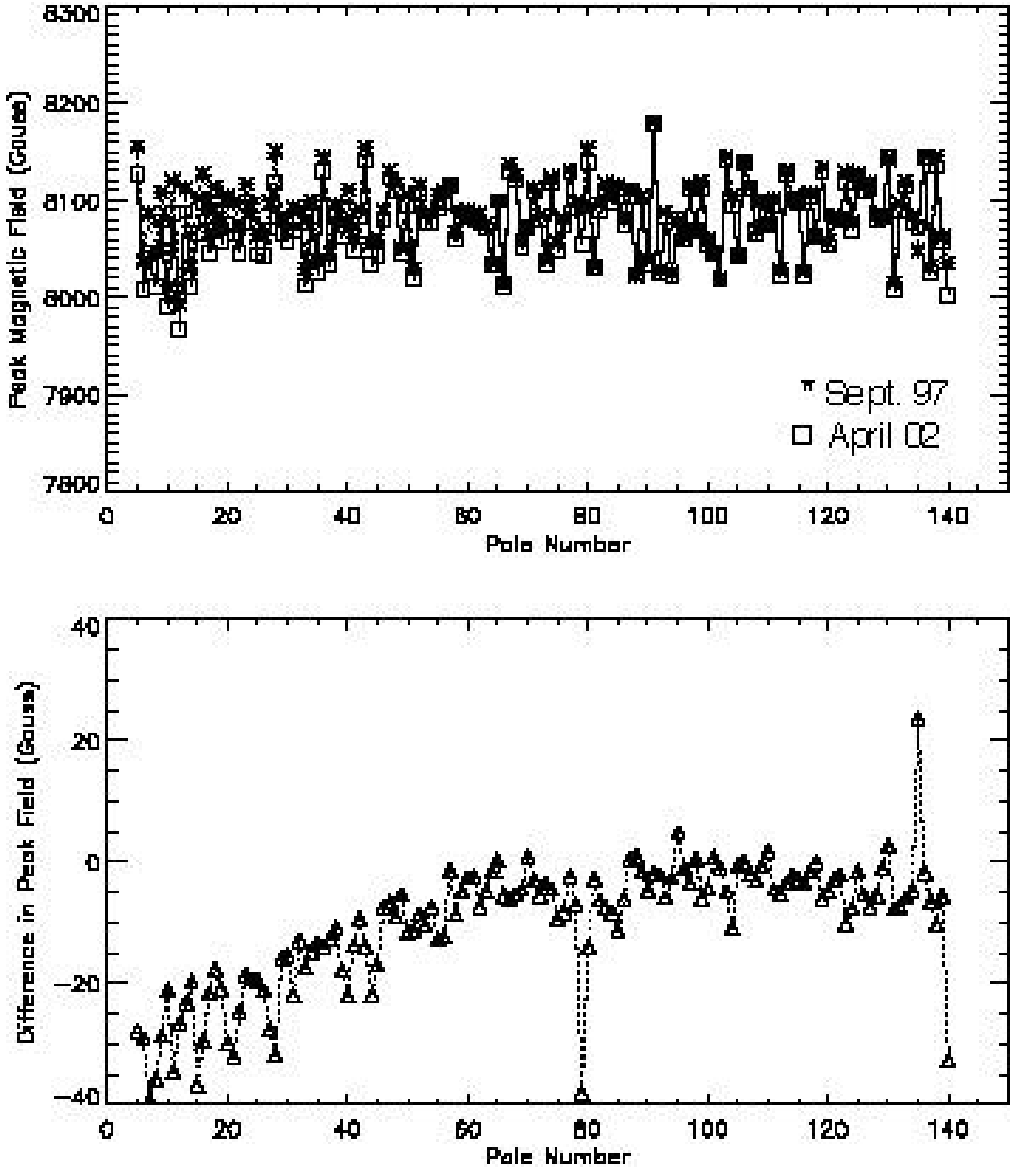

Fig. 2.6. Magnetic field changes in the downstream undulator in sector 1, U33#15, at 11.5 mm gap. The top panel shows the peak magnetic field under each pole as measured in Sept. 1997 and in April 2002. The bottom panel shows the difference in the magnetic field. (The data for the weaker end poles are omitted.) A slight decrease in field strength can be seen at the left, the downstream end.

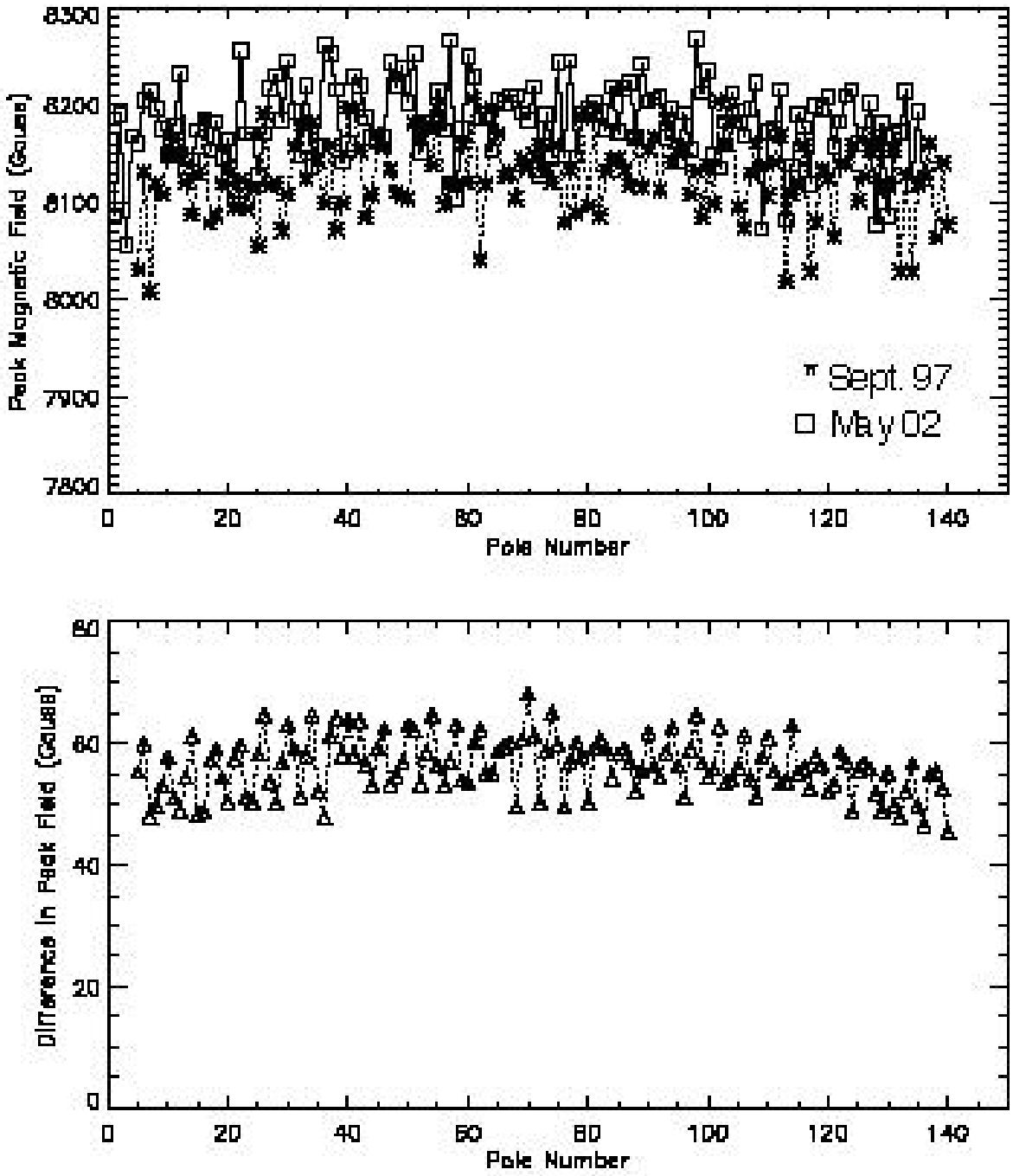

Fig. 2.7. An undamaged undulator! Magnetic field changes in the downstream undulator in sector 15, U33#3, at 11.5 mm gap. The top panel shows the peak magnetic field under each pole as measured in Sept. 1997 and in May 2002. The bottom panel shows the difference in the magnetic field. (The data for the weaker end poles are omitted.) There is no effective tapering of the field strength as was seen in the damaged devices. The overall increase in the field strength can be attributed to either a smaller Hall probe that integrates over a smaller region, thereby giving a higher peak field, or to improper removal of backlash in the gap-control mechanism.

The damage that can be seen in Figs. 2.3 – 2.6 includes, as a significant part, an effective taper in the magnetic field. Such a taper increases the rms phase errors and has a strong effect on the brilliance in the higher harmonics. Table 2.1 below shows the rms phase errors measured for each of the undulators initially, after the damage was observed, and after the device was retuned. An important part of the retuning consisted of altering the zero positions on the encoder position readouts in the undulator drive system to correct for the effective taper. The amount of the mechanical taper introduced is also shown in Table 2.1. The third harmonic of the undulator radiation, as calculated from the measured magnetic field, is given in the table as a percentage of the ideal intensity that would be obtained from a perfect undulator. (The original undulator specification aimed at having the third-harmonic intensity be at least 70% of ideal.) The radiation damage seen in the two undulators in sector 3 had a particularly strong effect on this third-harmonic intensity. The magnetic tuning was not able to remove all the damage from the downstream undulator. Instead, more extensive repair to this undulator will be needed.

Table 2.1. rms phase errors for specific undulators initially, after observed damage, and after retuning.

U27#12	**Gap 10.5 mm**		**Sector 3 DS**
Date	RMS Phase error	3rd harm., % of ideal	comment
1997 June 23	5.45	82.6	reference
2001 Dec. 31	36.5	35.2	damaged
2002 Jan. 3	9.29	69.0	tuned, taper 0.160mm
2002 May 6	14.14	52	more damage
2002 May 7	10.81	62.4	tuned, taper 0.025mm

U33#15	**Gap 11.5 mm**		**Sector 1 DS**
1997 Sept. 9	2.88	89.8	reference
2002 May 2	5.91	82	some damage
2002 May 3	5.14	84	tuned, taper 0.040 mm

APS27#2	**Gap 11.5 mm**		**Sector 3 US**
2000 June 23	2.62	91.5	reference
2002 Jan. 8	10.79	64.2	damaged
2002 Jan. 8	3.67	86.1	tuned, taper 0.150 mm

U33#3	**Gap 11.5 mm**		**Sector 15 DS**
1997 Sept.	4.54	91	reference
2002 May	5.14	89	still OK

2.1.3 Magnetic Measurement of the LCLS Prototype Undulator

Currently, an LCLS prototype undulator is under construction. The prototype is a 3.4-m-long hybrid-type undulator with a fixed gap of 6 mm. The period length is 30 mm, and the number of poles is 226. About 450 NdFeB magnet blocks will be used for this undulator. The requirements for integrated multipole moments are not demanding for this device, but those for trajectory straightness and for uniformity of the field strength at the beam position (undulator axis) are. All magnetic blocks received from Shin-Etsu have been investigated. For some magnets, the strength and direction of magnetization of the magnet blocks were measured using a Helmholtz-coil system and were compared with vendors results to confirm the validity. Hall probe measurements were performed for all magnet blocks while they were mounted in a specially designed fixture with Vanadium-Permendur poles. The magnet blocks were sorted using these data to minimize errors.

Figure 2.8 shows the variation of total magnetization. The maximum deviation from the average magnetization was smaller than ± 0.48%, and the standard deviation was 21 gauss (0.17%). Figure 2.9 shows a histogram of the magnet population. Although these numbers well exceed the specification, we applied a simple sorting for further improvement.

As shown in Fig. 2.9, the population distribution is symmetric about the average magnetization. Therefore, we chose pairs of magnets by matching the magnets at symmetric positions. Figure 2.10 shows the matched result. The pair of magnets will be mounted opposite one another in the assembled undulator (i.e., one in the top jaw, the other in the same position in the bottom jaw). If the stronger of the pair of magnets is placed in the upper jaw for this pair, then, for the adjacent pair of magnets in the undulator, the stronger will be in the lower jaw.

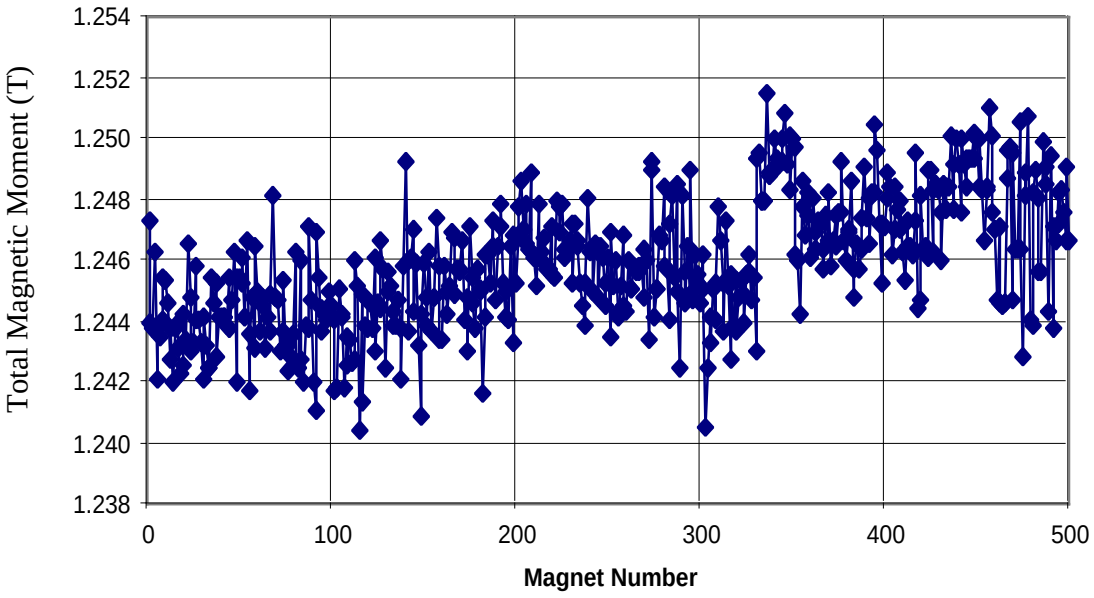

Fig. 2.8. Total magnetization as received.

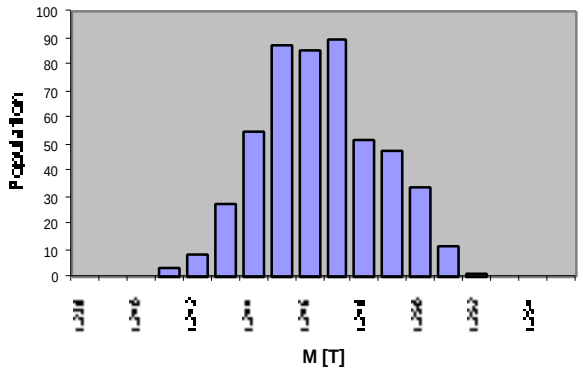

Fig. 2.9. Histogram of magnetization population.

The vertical scale of Fig. 2.10 is the same as that of Fig. 2.8 for easy comparison. The standard deviation after matching is only 1.24 Gauss (0.01%).

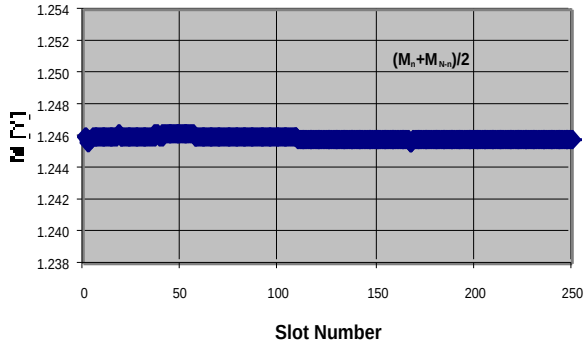

Fig. 2.10. Averaged magnetization after matching.

2.1.4 Improvements to the Magnetic Measurement Facility

The Magnetic Measurement Facility (MMF) includes systems to map the field of assembled IDs and to measure the magnetic strength of individual magnet blocks. These systems were built about 10 years ago, and some components, like computers, stepper motor controls, and analog integrators, have now become obsolete. Replacing them with fast ADCs, servomotors and up-to-date computers allowed improvement of the measurement capability while dispensing with long power cables whose excessive noise interfered with the measured signal. New control programs allow more sophisticated data analysis and representation and a more convenient user interface. The upgrade will increase the reliability and ease of maintenance, and aid future developments and possible duplication in other projects.

Stretched Coil Measurement System

A stretched coil that can be rotated or translated is used for precise measurements of magnetic field integrals and multipole components of different types of IDs (Deriy et al., 2001). In the new system, a fast ADC is used to acquire about 1000 data points per coil turn. This allows for more detailed analysis and better accuracy than the previous four points/turn. Error sources present in the coil signal, such as coil vibrations, can now be analyzed. Other changes were to reduce the number of crates and to move data acquisition and control into the computer case. The computer runs the Linux OS instead of Windows, which allows standard APS software modules to be adopted. The data format used widely at the APS, SDDS, is now used for the acquired data.

In the new system, a translation mode of measurement can be used to measure the integrated multipole components of the magnetic field more quickly than the previous rotation mode. There is also a mode for AC field integral measurements with improved time resolution and different triggering options.

Hall Probe Measurement System

A Hall probe that is moved through the ID gap is used to measure the spatial distribution of the magnetic field. This system includes the Hall probe readout, motors for positioning the Hall probe,

position readouts, triggers, and software for processing the data and displaying the results. The updating of this system is now in progress. A significant improvement will come from the change to motors with integral controllers, because the long wires that have been a source of electromagnetic noise in the measurements will be eliminated.

Helmholtz Coil System for Measurement of Individual Magnet Blocks

The Helmholtz coil system is used for measuring the direction and strength of the total magnetic moment of permanent magnet blocks. Each magnet block that is used in an undulator magnetic structure is measured individually, and the data are used to sort the magnet blocks and determine their arrangement in the assembled device.

The controls and readout of the system have been improved. The old analog integrator was replaced by a fast 16-bit National Instruments ADC on the PCI bus. The integration is now performed digitally. The old electronically noisy stepper motor has been replaced with a servomotor that incorporates electronics for servo-loop feedback. Previously, the magnet block was rotated in 15° steps, but now the measurements are made on-the-fly with a 10 kHz sampling rate. The result is a better signal/noise ratio and more data per turn for precise digital analysis. With the first set of magnets measured after the upgrade, a reproducibility of 3 parts in 10000 was achieved.

2.2 Synchrotron Radiation Instrumentation Engineering

The XFD develops instrumentation, beamline components, and front-end components, for SRI CAT, for other CATs, and for the APS facility.

2.2.1 Front-End Design for a Canted Undulator Beamline

The XFD has designed a front end for two canted undulator beamlines from a single straight section that will allow greater utilization of the APS (see Fig. 2.11). This design will be used in three new sectors. This front end, vs. 200c, is designed to operate at a maximum beam current of 200 mA with dual 2.07-m-long undulators with a 1 mrad x-ray beam separation at 10.5 mm ID gap (K=2.8). The maximum total power on the front end is 20 kW, and the maximum peak power density is 276 kW/mrad^2. Many innovations were made in this front-end design to improve performance and to reduce cost. Figure 2.12 shows a model of the photon shutter (PS1 and PS2). The design was the result of optimizing the cooling and cross section to reduce the mechanical stress from thermal loading. Another redesigned component was the safety shutter. The tungsten block was changed to simplify the geometry to reduce fabrication cost. The wall collimator was also redesigned and the length reduced from 800 mm to 300 mm, which simplifies installation while maintaining adequate shielding thickness. The sizes of most in-line vacuum fittings, such as the tubes and flanges, were reduced—significantly lowering the cost. Most of the pumps are mounted in-line to increase the pumping speed. All of the support tables were redesigned using commercially available extruded aluminum bars to reduce cost.